

Superconductivity driven by the screening of long-distance Coulomb interaction

Kosuke Odagiri

*Electronics and Photonics Research Institute, National Institute of Advanced Industrial Science and Technology,
Tsukuba Central 2, 1-1-1 Umezono, Tsukuba, Ibaraki 305-8568, Japan*

(Dated: March 1, 2022)

The pair-fluctuation contribution reduces the electrostatic screening length in superconductivity as compared to the normal state. When a conductor possesses a static background charge distribution, superconductivity arises even in the absence of an explicit pairing interaction, such that the Coulomb repulsion is reduced and the total energy is lowered. We demonstrate that the superconducting gap increases with increased background charge at first, after which the mixing of the Higgs and plasma modes suppresses superconductivity in the pseudogap phase. This indicates that the mechanism may be relevant to the cuprates and iron pnictides. When the background charge is identified with the incoherent component of optical conductivity in the cuprates, our results reproduce the shape, size and position of the superconducting dome with zero free parameters. A superconducting critical temperature of about 1000 K is possible in ion-doped conductors.

INTRODUCTION

In this letter, we propose and explore a novel mechanism of SC ('superconductivity' or 'superconducting'), where SC is driven by charge-screening.

Quite surprisingly, this mechanism seems able to explain the universal features of the unconventional superconductors such as the cuprates [1, 2] and the iron pnictides [3], quantitatively without free parameters. By 'universal features', we mean: 1. small amount of carrier- or charge-doping creates an SC 'dome'; 2. the maximum T_c (transition temperature) is correlated with electronic energy scales such as the characteristic temperature T_0 of spin fluctuation [4] or more simply $W/(m_*/m)$ where W is proportional to the bandwidth and m_* is the effective mass at the Fermi level [5]; 3. there is an 'underdoped' pseudogap state.

Our mechanism is based on the reduction, typically by $\sim 10\%$, of the electrostatic screening length in the SC phase. This is caused by pair fluctuation, which is calculated as loops of Higgs and Goldstone bosons, shown in Fig. 1. This effect is not surprising, because the SC condensate contributes extra degrees of freedom to charge screening compared to the normal state.

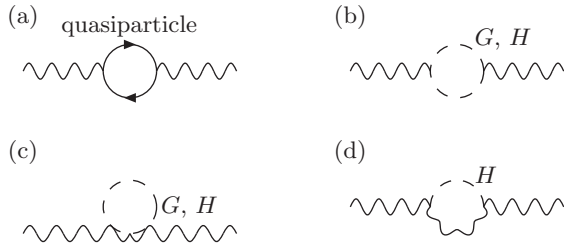


FIG. 1. The diagrams for the self-energy of the photon (curly lines). Diagram (d) is zero by choice of gauge. Photonic tadpole graph, which is omitted here, is also zero by the choice of gauge

A conductor that contains an unbalanced and static background charge distribution ρ_s will therefore become SC such that the net Coulomb repulsion is reduced. The charge distribution ρ_s may be either ionic, or due to some charge carrier that is immobilized by, e.g., spin or orbital interaction.

Diagrammatically speaking, the energy gain due to this effect is described by Fig. 2a. This needs to be balanced by the more conventional contributions of Figs. 2b, c. There is also a self-energy contribution of Fig. 2d.

The gap Δ_{SC} increases with increased ρ_s at first, after which the contribution of Fig. 2e causes Higgs-plasma mixing and suppresses SC. The latter phase corresponds to the pseudogap, where SC pairs are formed for a short time but are trapped and dissolved by the background charge.

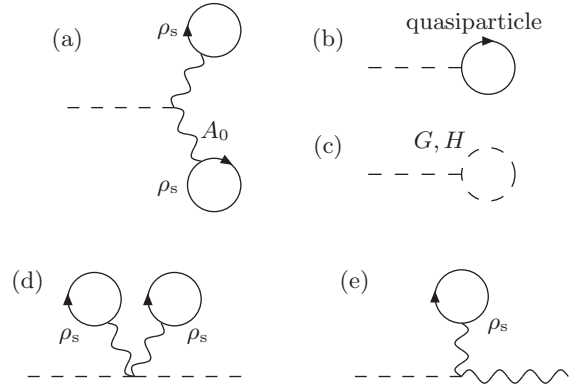


FIG. 2. The 'slug' (a), the quasiparticle (b) and bosonic (c) contributions to the Higgs tadpole; new contribution to the Higgs self-energy (d); and the Higgs-photon (plasmon) mixing diagram (e). ρ_s refers to the background charge

Our calculation is based on nonperturbative (quasi-perturbative) one-loop self-consistency conditions of the long-distance Higgs and Goldstone modes, and has essentially zero free parameters.

The results of our calculation in the two-dimensional (2-d) case are consistent with the experimental findings, provided that the ‘incoherent’ component [6] of optical conductivity acts as ρ_s . The size, position and shape of the SC dome are reproduced.

For the three-dimensional (3-d) case, because of the smaller size of SC fluctuation, the SC gap will be nearly three times greater than the 2-d case and will typically be $\mathcal{O}(0.1 \text{ eV})$. The fabrication of a bulk material with charge imbalance will be a technological challenge. For proof-of-principle studies, a more practical alternative will be to study surface conductivity under applied electric field [7].

DEFINITIONS AND CALCULATIONAL SETUP

The SC gap is defined by:

$$\mathcal{L} = -\Psi^\dagger \begin{pmatrix} \xi(\mathbf{k}) & e^{-i\phi_{\text{SC}}} \Delta_{\text{SC}} \\ e^{+i\phi_{\text{SC}}} \Delta_{\text{SC}} & -\xi(-\mathbf{k}) \end{pmatrix} \Psi. \quad (1)$$

We adopt $\phi_{\text{SC}} = 0$ without loss of generality. Ψ is the Nambu doublet [8], and is parametrized in terms of the lower and upper quasiparticle bands as:

$$\Psi = \begin{pmatrix} \psi_\uparrow \\ \psi_\downarrow \end{pmatrix} = \begin{pmatrix} \cos \theta_{\text{SC}} & -\sin \theta_{\text{SC}} \\ \sin \theta_{\text{SC}} & \cos \theta_{\text{SC}} \end{pmatrix} \begin{pmatrix} u \\ \ell \end{pmatrix}. \quad (2)$$

Equation (1) is diagonalized by mixing angle θ_{SC} given by

$$\tan 2\theta_{\text{SC}}(\mathbf{k}) = \Delta_{\text{SC}}/\xi(\mathbf{k}), \quad (-\pi/4 \leq \theta_{\text{SC}} \leq +\pi/4). \quad (3)$$

We generalize eqn. (1) by including the Higgs and Goldstone degrees of freedom. We introduce the following parametrization:

$$\Phi_{\text{SC}} = (v + H)\sigma_1 + G\sigma_2. \quad (4)$$

v is the Higgs-boson vacuum expectation value. σ are the Pauli matrices. G corresponds to the broken part of the vectorial $U(1)$ symmetry under

$$\Psi \rightarrow e^{i\theta_V \sigma_3} \Psi, \quad (5)$$

whereas H corresponds to the conserved axial $U(1)_A$ symmetry under

$$\Psi \rightarrow e^{i\theta_A} \Psi. \quad (6)$$

The interaction of the Higgs and Goldstone bosons with fermions is given by the following generalization of the off-diagonal part of eqn. (1):

$$\mathcal{L}_{\Phi\psi\psi} = -v^{-1} \Delta_{\text{SC}} \Psi^\dagger \Phi_{\text{SC}} \Psi. \quad (7)$$

H and G kinetic terms are parametrized by

$$\begin{aligned} \mathcal{L}_{\text{kin}} = & \frac{1}{4} \text{Tr} \left| \left(i\hbar \frac{\partial}{\partial t} + 2eA_0\sigma_3 \right) \Phi_{\text{SC}} \right|^2 \\ & - \frac{u^2}{4} \text{Tr} |(-i\hbar\nabla + 2e\mathbf{A}\sigma_3) \Phi_{\text{SC}}|^2, \end{aligned} \quad (8)$$

e is positive in our convention. This is similar to the standard Ginzburg–Landau formulation where the one-component order-parameter Φ_{GL} is proportional to $(v + H) + iG$, and has the advantage that the unphysical H – A_0 mixing term is absent.

After the symmetry breaking, the electrostatic plasma mode develops an energy gap $\Delta_{A_0} = 2ev$, whereas the magnetic mode acquires an energy gap $\Delta_{\mathbf{A}} = 2(u/c)ev$, which corresponds to the penetration depth $\lambda_{\text{SC}} = c/\Delta_{\mathbf{A}} = c^2/2uev$.

The symmetry-breaking potential is assumed to be of the form

$$V = (\Delta_H^2/8v^2) [G^2 + (H + v)^2 - v^2]^2. \quad (9)$$

Δ_H is the excitation energy of the Higgs mode, and is related to the coherence length by

$$\xi_{\text{SC}} = u\hbar\sqrt{2}/\Delta_H. \quad (10)$$

Equation (8) contains the following bilinear terms:

$$2ev \left[A_0 \frac{\partial G}{\partial t} + u^2 \mathbf{A} \cdot \nabla G \right]. \quad (11)$$

We cancel these up to total derivatives by adding ‘t Hooft gauge-fixing terms:

$$- \frac{1}{2\xi_g} \left(\frac{\partial A_0}{\partial t} + u^2 \nabla \cdot \mathbf{A} - 2ev\xi_g G \right)^2. \quad (12)$$

The subscript g refers to gauge-fixing. For the situations concerning gauge-fixing in ordinary time-dependent Ginzburg–Landau theory, see, e.g., ref. [9].

The Goldstone and Higgs propagators are now given by

$$D_G(E, \mathbf{k}) = (E^2 - u^2 \mathbf{k}^2 - \xi_g \Delta_{A_0}^2 + i0)^{-1}, \quad (13)$$

$$D_H(E, \mathbf{k}) = (E^2 - u^2 \mathbf{k}^2 - \Delta_H^2 + i0)^{-1}. \quad (14)$$

The Goldstone-boson excitation energy $\xi_g^{1/2} \Delta_{A_0}$ vanishes when $\xi_g \rightarrow 0$. Since physical quantities should not depend on the gauge choice, let us choose this particular limit. This corresponds to assigning all longitudinal component of A_μ to G , where being longitudinal refers to being proportional to $(q_0, (u/c)^2 \mathbf{q}) \approx (q_0, \mathbf{0})$. In other words, A_0 is now described by G whereas \mathbf{A} is small for our purposes. This is with the exception of the case of A_0 coupling to a conserved electromagnetic current such as ρ_s , in which case the A_0 mode will propagate because the longitudinal coupling to ρ_s gives zero.

The Goldstone-boson contribution will yield logarithmic divergences in the 2-d case at finite temperatures in accordance with the Coleman–Mermin–Wagner theorem. We shall only study 2-d and 3-d systems at zero temperature here.

The interaction Feynman rules are given by $i\mathcal{L}$, and are listed in Tab. I.

Vertex	Feynman rule
$u_1^\dagger \ell_2 G, \ell_1^\dagger u_2 G$	$\mp v^{-1} \Delta_{\text{SC}} \cos(\theta_1 - \theta_2)$
$u_1^\dagger u_2 G, \ell_1^\dagger \ell_2 G$	$\pm v^{-1} \Delta_{\text{SC}} \sin(\theta_1 - \theta_2)$
$u_1^\dagger \ell_2 H, \ell_1^\dagger u_2 H$	$-iv^{-1} \Delta_{\text{SC}} \cos(\theta_1 + \theta_2)$
$u_1^\dagger u_2 H, \ell_1^\dagger \ell_2 H$	$\mp iv^{-1} \Delta_{\text{SC}} \sin(\theta_1 + \theta_2)$
$u_1^\dagger \ell_2 A_0, \ell_1^\dagger u_2 A_0$	$-ie \sin(\theta_1 + \theta_2)$
$u_1^\dagger u_2 A_0, \ell_1^\dagger \ell_2 A_0$	$\pm ie \cos(\theta_1 + \theta_2)$
GGH	$-iv^{-1} \Delta_H^2$
HHH	$-3iv^{-1} \Delta_H^2$
$GGHH$	$-iv^{-2} \Delta_H^2$
$GGGG, HHHH$	$-3iv^{-2} \Delta_H^2$
$A_0 A_0 H$	$+iv^{-1} \Delta_{A_0}^2$
$\mathbf{A} \mathbf{A} H$	$-iv^{-1} \Delta_{\mathbf{A}}^2$
$A_0 A_0 GG, A_0 A_0 HH$	$+iv^{-2} \Delta_{A_0}^2$
$\mathbf{A} \mathbf{A} GG, \mathbf{A} \mathbf{A} HH$	$-iv^{-2} \Delta_{\mathbf{A}}^2$
$A_0 GH$	$v^{-1} \Delta_{A_0} E_G$
$\mathbf{A} GH$	$-v^{-1} u \Delta_{\mathbf{A}} \mathbf{k}_G$

TABLE I. Interaction Feynman rules

ELECTROSTATIC CHARGE SCREENING

Let us calculate v by calculating the self-energy of A_0 . The relevant Feynman diagrams are shown in Fig. 1. We are interested mainly in the case of zero external energy and momenta, which corresponds to calculating the long-distance screening length.

The contribution of Fig. 1a to v^2 is given by

$$4v_{(a)}^2 = 2i \int \frac{d^{d+1}k}{(2\pi)^{d+1}} (\sin 2\theta_{\text{SC}}(\mathbf{k}))^2 G_u(k) G_\ell(k) \quad (15)$$

at zero external 4-momenta. Since the u states are empty and ℓ states are occupied, we obtain

$$v_{(a)}^2 = \frac{1}{4} \int \frac{d^d \mathbf{k} (\sin 2\theta_{\text{SC}}(\mathbf{k}))^2}{(2\pi)^d \sqrt{\Delta_{\text{SC}}^2 + \xi^2}} \approx \frac{g_F}{4}, \quad (16)$$

where g_F is the normal-state density of states at the Fermi surface. The charge screening due to the quasi-particle loop is, as is well known, the same as the normal-state Fermi–Thomas screening.

The contribution of Fig. 1b is given by

$$\begin{aligned} v_{(b)}^2 &= i \int \frac{d^{d+1}k}{(2\pi)^{d+1}} k_0^2 D_G(k) D_H(k) \\ &= \frac{1}{2\Delta_H^2} \int \frac{d^d \mathbf{k}}{(2\pi)^d} \left[\sqrt{u^2 \mathbf{k}^2 + \Delta_H^2} - u |\mathbf{k}| \right]. \end{aligned} \quad (17)$$

We shall discuss the momentum cutoff of the integrals in due course. The parameter u is calculable by evaluating the self-energies of G and H at finite spatial momenta, with the result that $u \approx v_F$ where v_F is the Fermi velocity. We shall omit the details here.

The following approximation and parametrization are convenient:

$$v_{(b)}^2 \approx \frac{1}{8} \int \frac{d^d \mathbf{k}}{(2\pi)^d} \left[\frac{1}{u |\mathbf{k}|} + \frac{1}{\sqrt{u^2 \mathbf{k}^2 + \Delta_H^2}} \right] = \frac{g_G + g_H}{4}. \quad (18)$$

The third contribution is given by

$$v_{(c)}^2 = \frac{i}{2} \int \frac{d^{d+1}k}{(2\pi)^{d+1}} [D_G(k) + D_H(k)] = \frac{g_G + g_H}{2}. \quad (19)$$

Hence

$$v^2 = v_{(a)}^2 + v_{(b)}^2 + v_{(c)}^2 \approx (g_F + 3g_G + 3g_H)/4. \quad (20)$$

THE MECHANISM OF SUPERCONDUCTIVITY

In conventional superconductivity [10, 11], one representation of the gap equation is the following all-order equation:

$$\Delta_{\text{SC}} = \psi_\uparrow \rightarrow \text{1PI} \leftarrow \psi_\downarrow^* + \Delta_{\text{SC}}^{\text{bare}}. \quad (21)$$

The blob contains all one-particle irreducible contributions. Since Δ_H is generated dynamically, the all-order versions of Figs. 2b, c cancel automatically provided $\Delta_{\text{SC}}^{\text{bare}} \rightarrow 0$. This justifies the conventional prescriptions.

Let us consider the case where there is no direct pairing interaction as such, and SC is stabilized by Fig. 2a. We then obtain $\Delta_{\text{SC}} = \Delta_{\text{SC}}^{\text{bare}}$, and Δ_{SC} is now determined by the cancellation of Figs. 2a, c, which minimizes the ground-state energy. The contribution of Fig. 2b is zero to the leading order.

Let us carry out this programme. Figure 2a gives the energy gain due to screening:

$$\mathcal{A}_{(a)} = -\frac{1}{2} v^{-1} \Delta_{A_0}^2 \left(\frac{1}{\Delta_{A_0}^2} \right)^2 (\rho_s e)^2 = -\frac{v^{-3} \rho_s^2}{8}. \quad (22)$$

Figure 2c gives the energy loss due to bosonic Casimir energy or, in other words, SC fluctuation:

$$\begin{aligned} \mathcal{A}_{(c)} &= -\frac{1}{2} \int \frac{d^{d+1}k}{(2\pi)^{d+1}} v^{-1} \Delta_H^2 (D_G(k) + 3D_H(k)) \\ &= v^{-1} \Delta_H^2 (g_G + 3g_H)/2. \end{aligned} \quad (23)$$

Therefore the equilibrium condition is

$$\frac{\rho_s^2}{g_F + 3g_G + 3g_H} = (g_G + 3g_H) \Delta_H^2. \quad (24)$$

H and A_0 states mix through the process shown in Fig. 2c. The contribution equals $ev^{-1} \rho_s$, and so the H – A_0 mass matrix is given by

$$\frac{1}{2} (H \ A_0) \begin{pmatrix} \Delta_H^2 & ev^{-1} \rho_s \\ ev^{-1} \rho_s & \Delta_{A_0}^2 \end{pmatrix} \begin{pmatrix} H \\ A_0 \end{pmatrix}. \quad (25)$$

We redefined A_0 as positive norm here for the sake of convenience.

After diagonalization, the rotated Δ_H^2 is given by

$$\Delta_{H'}^2 = \Delta_H^2 - v^{-4} \rho_s^2 / 4. \quad (26)$$

We used $\Delta_{A_0}^2 \gg \Delta_H^2$. Hence

$$\Delta_H^2 = \frac{v^{-2} \rho_s^2}{4g_G + 12g_H}, \quad \Delta_{H'}^2 = \frac{v^{-4} \rho_s^2 (v^2 - g_G - 3g_H)}{4g_G + 12g_H}. \quad (27)$$

To proceed further, we need to determine the cutoff of the integrals in g_G, g_H . This can be done by evaluating Δ_H at finite momenta. In general, Δ_H is calculated using self-energy diagrams of Fig. 3 and Fig. 2d. The contributions are individually divergent, but the sum is finite (except the long-distance and imaginary divergence of Fig. 3b) so long as the tadpoles of Figs. 2a, b, c cancel.

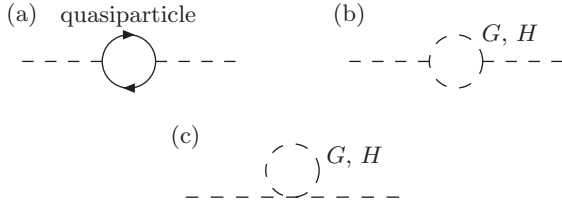


FIG. 3. The diagrams for the self-energy of the Higgs (and Goldstone) boson

After the cancellations take place, and at zero momentum, we obtain

$$\Delta_H^2(0) = g_F \int d\xi \frac{(v^{-1} \Delta_{SC} \sin 2\theta_{SC})^2}{\sqrt{\Delta_{SC}^2 + \xi^2}} = g_F v^{-2} \Delta_{SC}^2. \quad (28)$$

One way to generalize this to finite momenta is to calculate the difference of Higgs and Goldstone self-energies [12]:

$$\Delta_H^2(q) = \Sigma_H(q) - \Sigma_G(q). \quad (29)$$

The dominant contribution is due to Fig. 3a. This leads to a simple generalization of eqn. (28):

$$\Delta_H^2(0, \mathbf{q}) = g_F \int d\xi \frac{(v^{-1} \Delta_{SC})^2 \sin 2\theta_{SC} \langle \sin 2\theta'_{SC} \rangle}{\sqrt{\Delta_{SC}^2 + \xi^2}}. \quad (30)$$

Here $\tan 2\theta_{SC} = \Delta/\xi(\mathbf{k})$ whereas $\tan 2\theta'_{SC} = \Delta/\xi(\mathbf{k} + \mathbf{q})$. $\langle \dots \rangle$ denotes the average over the solid angle of \mathbf{k} . For small \mathbf{q} and an isotropic density of states, we obtain

$$\Delta_H^2(0, \mathbf{q}) \propto \left\langle \text{Im} \left[\frac{\sin^{-1} \sqrt{z/2i}}{z\sqrt{1-2i/z}} \right] \right\rangle, \quad (31)$$

where $z = v_F |\mathbf{q}| \cos \phi / \Delta_{SC}$. ϕ is the azimuthal angle of \mathbf{q} with respect to \mathbf{k} . We integrate over the solid angle numerically, and obtain the results shown in Fig. 4. The curves fall as $1/|\mathbf{q}|$ at large \mathbf{q} . We see that the half-width is approximately 6 for 2-d and 8 for 3-d. We shall use these numbers to estimate the cutoff.

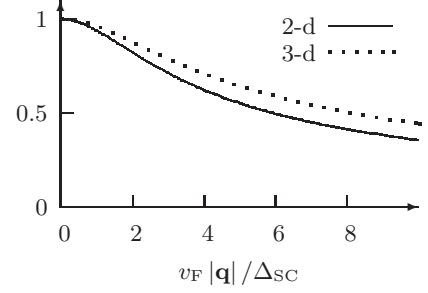


FIG. 4. $\Delta_H^2(0, \mathbf{q})/\Delta_H^2(0)$ as a function of $v_F |\mathbf{q}|/\Delta_{SC}$

RESULTS

Let us now return to eqn. (27).

We introduce a simple cutoff at $u |\mathbf{k}| = c \Delta_H$ in g_G . Here $c \approx 6$ for 2-d and ≈ 8 for 3-d. As c is sufficiently large, $g_H = g_G$ to a good approximation. We obtain

$$g_G, g_H = \begin{cases} c \Delta_H / 4\pi u^2 & (2\text{-d}), \\ c^2 \Delta_H^2 / 8\pi^2 u^3 & (3\text{-d}). \end{cases} \quad (32)$$

This implies

$$\Delta_H = \begin{cases} (u^2 \rho_s^2 / 4c v^2)^{1/3} & (2\text{-d}), \\ (u^3 \rho_s^2 \pi^2 / 2c^2 v^2)^{1/4} & (3\text{-d}). \end{cases} \quad (33)$$

For SC to be stable, we need $\Delta_{H'}^2 > 0$. This implies $g_F > g_G + 9g_H$. Therefore, crudely speaking, $v^2 \approx g_F/4$ by eqn. (20), and $\Delta_H \approx 2\Delta_{SC}$ by eqn. (28). There are thus two gaps, $2\Delta_{SC} \approx \Delta_H > \Delta'_H$. It is natural to associate the former gap with the pseudogap. In this pseudogap phase, SC decays by coupling with ρ_s .

Let us define $x_s = \rho_s/\rho_1$, where

$$\rho_1 = \begin{cases} (2\pi/c)(uv^2)^2 & (2\text{-d}), \\ (\pi/c)(2uv^2)^{3/2} & (3\text{-d}). \end{cases} \quad (34)$$

We then obtain

$$\Delta_{H'} = \frac{\rho_1}{2v^2} \times \begin{cases} x_s^{2/3} \sqrt{1 - x_s^{2/3}} & (2\text{-d}), \\ \sqrt{x_s(1 - x_s)} & (3\text{-d}). \end{cases} \quad (35)$$

Adopting the approximation $v^2 \approx g_F/4$, there is thus a universal overall behaviour for each number of dimensions as shown in Fig. 5.

For the sake of estimation, let us adopt

$$(4v^2)u \approx g_F v_F \approx \begin{cases} k_F/\pi \approx 1/a & (2\text{-d}), \\ k_F^2/\pi^2 \approx 1/a^2 & (3\text{-d}). \end{cases} \quad (36)$$

This yields

$$\rho_1 \approx \begin{cases} 0.065/a^2 & (2\text{-d}), \\ 0.14/a^3 & (3\text{-d}). \end{cases} \quad (37)$$

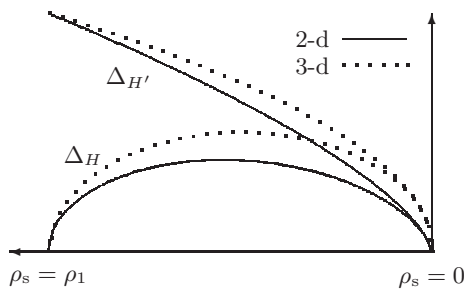


FIG. 5. Δ_H and $\Delta_{H'}$ as function of ρ_s (increases towards the left) in the 2-d and 3-d systems. With arbitrary normalization

We used $c = 6$ for 2-d and 8 for 3-d. From Fig. 4, there is approximately 50 % uncertainty in the values of c and hence in these numbers.

Let us compare the results with the phenomenology in the 2-d case. For the cuprates, SC sets in at a doping of typically 0.05 to 0.07 per unit cell, and it has been found that at low doping, most of the doped carriers are ‘incoherent’ [6]. Supposing that these ‘incoherent’ carriers are to be identified with ρ_s , these numbers agree well with $0.065/a^2$ derived above. SC in the cuprates disappears when the ‘incoherent’ carriers vanish. This corresponds to $\rho_s = 0$, and is again in agreement with the theory.

As for the overall magnitude, let us define $uk_F \approx 2W_{\text{eff}}$, the effective electronic energy scale as estimated at the Fermi level. We then obtain

$$\Delta_{H'}^{\text{max}} \approx \begin{cases} 0.032W_{\text{eff}} & (2\text{-d}), \\ 0.088W_{\text{eff}} & (3\text{-d}). \end{cases} \quad (38)$$

For the cuprates, $W_{\text{eff}} \sim 0.1$ eV, and so the gap and hence T_c is $\mathcal{O}(50\text{ K})$, which agrees with the phenomenology. The universal correlation of T_c with W_{eff} is a well-known feature of a class of superconductors which includes the cuprates and iron pnictides.

DISCUSSION

The size of the coefficients in eqn. (38) suggests that it will be surprisingly easy to achieve room-temperature SC. For $W_{\text{eff}} = 1$ eV for example, we would expect a maximum T_c of about 1000 K in 3-d systems.

The major factor which suppresses W_{eff} and hence T_c at present is the large size of the effective mass m_* . m_* is typically large because the physics which creates the static trapped charge carriers ρ_s also slows down the dynamical charge carriers.

This situation needs not be the case in general, if our discussions have been correct. One can create ρ_s more simply as impurity ions.

For proof-of-principle studies, the simplest method would be to use an external electric field and study surface SC in 3-d bulk conductors that are doped with ions. The technology that is necessary for such a study will be similar to that adopted in the context of electric-field-induced SC [7]. One would simply need to substitute an ion-doped conductor for SrTiO_3 that is studied in ref. [7]. The thickness of the surface layer will be governed by the screening length of the Coulomb interaction.

As for the choice of the conductor, the only theoretical requirement is that the long-distance Coulomb interaction must not be suppressed. An isolated conduction band is therefore preferable, but d -band metals are permissible so long as the Fermi level is at the tail of the d -band, e.g., Cu or Zn. As for the dopant, ions that have the same sign of charge as the dynamical carriers would be preferable so as to avoid the trapping of dynamical carriers. For Cu, since the charge carriers are electrons, the dopant should be anions such as the halogens. For Zn, the dopant should be cations such as the alkali metals. The optimal doping concentration will be approximately 8 %.

CONCLUSIONS

The suppression of long-distance Coulomb interaction in the SC phase implies that a conductor that is doped with static background charge will become SC in order that the total energy of the system is minimized. We studied this mechanism by utilizing a modified tadpole-cancellation condition.

The SC gap increases with increasing background charge up to a certain point, after which SC is suppressed in the pseudogap phase when the mixing between the electrostatic plasmon field and the Higgs mode suppresses SC.

The results are quantitatively consistent with the phenomenology for 2-d systems. 3-d systems will exhibit higher T_c and will be candidates for room-temperature superconductivity.

A further test of our mechanism will be the measurement of Higgs–plasmon mixing by optical emission, but this will be difficult because of the large size of the decay width $\Gamma_{H'} \sim \Delta_{H'}$.

It would be interesting but challenging to amalgamate our long-distance formulation with a short-distance theory as, for instance, our theory cannot predict the pairing symmetry as it stands. This short-distance theory will be one that is equipped with a static charge distribution ρ_s and mobile charge carriers, together with some implementation of long-distance Coulomb interaction.

Acknowledgments: The author thanks the members of the Superconducting Electronics Group, AIST, as well as N. Yamada and K. Yamaji for their patience and support. A precursory work was carried out in 2012 at Pun-

jabi University, Patiala. We thank R. C. Verma and the supporting staff members of Punjabi University, Patiala, who made the visit possible.

-
- [1] J. G. Bednorz and K. A. Mueller, Z. Phys. **B64** (1986) 189.
 - [2] J. R. Schrieffer (ed.), *Handbook of High-Temperature superconductivity*, Springer, New York, 2007.
 - [3] D. C. Johnston, Adv. Phys. **59** (2010) 803.
 - [4] S. Nakamura, T. Moriya and K. Ueda, J. Phys. Soc. Jpn. **65** (1996) 4026.
 - [5] T. Yanagisawa, internal presentation, AIST, Tsukuba, April 2012; private communications.
 - [6] S. Uchida, T. Ido, H. Takagi, T. Arima, Y. Tokura and S. Tajima, Phys. Rev. **B43** (1991) 7942.
 - [7] K. Ueno, S. Nakamura, H. Shimotani, A. Ohtomo, N. Kimura, T. Nojima, H. Aoki, Y. Iwasa and M. Kawasaki, Nat. Mater. **7** (2008) 855.
 - [8] Y. Nambu, Phys. Rev. **117** (1960) 648.
 - [9] Q. Du, Appl. Anal. **53** (1994) 1.
 - [10] L. N. Cooper, Phys. Rev. **104** (1956) 1189; J. Bardeen, L. N. Cooper and J. R. Schrieffer, Phys. Rev. **106** (1957) 162, *ibid.* **108** (1957) 1175.
 - [11] A. A. Abrikosov, L. P. Gorkov and I. E. Dzyaloshinski, *Methods of Quantum Field Theory in Statistical Physics*, Dover Publications, New York, 1975.
 - [12] V. N. Gribov, Phys. Lett. **B 336** (1994) 243 [arXiv:hep-ph/9407269].